Remote sensing of lake water volumes on the Arctic Coastal Plain of Northern Alaska

Claire E. Simpson[1], Christopher D. Arp[2], Yongwei Sheng[1], Mark L. Carroll[3], Benjamin M.

Jones[2], Laurence C. Smith[1,4,5]

[1]Department of Geography, University of California, Los Angeles (UCLA), Los Angeles, California, 90095, USA
[2]Water and Environmental Research Center, University of Alaska, Fairbanks, 306 Tanana Loop Rd., Fairbanks, Alaska, 99775, USA
[3]Computational and Information Science and Technology Office, NASA-GSFC, Greenbelt, Maryland, 20771, USA
[4]Department of Earth, Environmental and Planetary Sciences, Brown University, 324 Brook St, Providence, Rhode Island, USA, 02912
[5]Institute at Brown for the Environment and Society, Brown University, 85 Waterman St, Providence, Rhode Island, USA, 02912

Correspondence to: Claire E. Simpson (clairesimpson17@gmail.com)

Abstract. The Pleistocene Sand Sea on the Arctic Coastal Plain (ACP) of northern Alaska is underlain by an ancient sand dune field, a geological feature that affects regional lake characteristics. Many of these lakes, which cover approximately 20% of the Pleistocene Sand Sea, are relatively deep (up to 25 m). In addition to the natural importance of ACP Sand Sea lakes for water storage, energy balance, and ecological habitat, the need for winter water for industrial development and exploration activities makes lakes in this region a valuable resource. However, ACP Sand Sea lakes have received little prior study. Here, we use in situ bathymetric data to test 12 model variants for predicting Sand Sea lake depth based on analysis of Landast-8 Operational Land Imager (OLI) images. Lake depth gradients were measured at 17 lakes in mid-summer 2017 using a HumminBird 798ci HD SI Combo automatic sonar system. The field measured data points were compared to Red-Green-Blue (RGB) bands of a Landsat-8 OLI image acquired on 8 August 2016 to select and calibrate the most accurate spectral-depth model for each study lake and estimate bathymetry. Exponential functions using a simple band ratio (with bands selected based on lake turbidity and bed substrate) yielded the most successful model variants. For each lake, the most accurate model explained 81.8% of the variation in depth, on average. Modeled lake bathymetries were integrated with remotely sensed lake surface area to quantify lake water storage volumes, which ranged from 1.056×10^{-3} km^3 to 57.416×10^{-3} km^3. Due to variation in depth maxima, substrate, and turbidity between lakes, a regional model is currently infeasible, rendering necessary the acquisition of additional in situ data with which to develop a regional model solution. Estimating lake water volumes using remote sensing will facilitate better management of expanding development activities and serve as a baseline by which to evaluate future responses to ongoing and rapid climate change in the Arctic. All sonar depth data and modeled lake bathymetry rasters can be freely accessed at https://doi.org/10.18739/A2SN01440 (Simpson and Arp, 2018) and https://doi.org/10.18739/A2TQ5RD83 (Simpson, 2019), respectively.

1 Introduction

The Arctic Coastal Plain (ACP) of Alaska is distinguished by the presence of thousands of lakes, many of which are the product of thermokarst processes (Hopkins, 1949). Thermokarst is the melting of ice in permafrost, resulting in thaw settlement and land surface subsidence (van Everdingen, 1998); such activity may lead to the development of thermokarst lakes (Hopkins, 1949; Jorgenson and Shur, 2007). While thermokarst lakes on the ACP

typically reach maximum depths between 1 to 3 m (Hinkel et al., 2012), an anomalous group of lakes on the ACP

45   approach depths up to approximately 25 m.

       Deep lakes that are the focus of this study are located on the Pleistocene Sand Sea (Fig. 1), a distinctive

region of the ACP named for its foundational Pleistocene-aged sand sheet and sand dunes (Carter, 1981; Williams,

1983; Williams et al., 1978). Located west of the Colville River, this region spans approximately 15,000 km^2 and

contains over 16,000 lakes (Jorgenson et al., 2014). The underlying dune field impacts the regional lithology and

50   lake morphology. Lakes here are nestled between the crests of sand dunes and display a form distinct from that of

lakes across the rest of Alaska's North Slope (Hinkel et al., 2005; Jorgenson and Shur, 2007). Deep central basins

and wide, shallow littoral shelves surrounded by bluffs distinguish Sand Sea lakes from lakes that have formed in

ice-rich permafrost terrain. Studies by Livingstone (1954), Rex (1961), Carson and Hussey, (1962), and Carson

(1968) assert that the supra-lake bluffs erode by winds, which carry sand from the bluff faces into the lakes, forming

55   characteristic sandy littoral shelves. These shelves only reach depths of up to three m, whereas the central basins of

such lakes can reach depths over eight times that. Due to this striking depth contrast, the distinction between littoral

shelves and central basins is apparent in satellite imagery of most lakes in the area (given low-wind and ice-free

conditions). Understanding the geological context and morphology of Sand Sea lakes is important when interpreting

their spectral signatures in remotely sensed imagery.

60   In this study, we (1) present a dataset to help fill the gap concerning lake depth - particularly deep lake

depth - measurements in Arctic regions, (2) leverage the dataset to tune linear spectral-depth models at individual

lakes for the purpose of lake-wide bathymetry mapping, and (3) integrate the modeled depths across each lake to

quantify water volumes. Finally, we assess spectral-depth similarity in lakes across the Sand Sea to evaluate the

prospects of regional water volume modeling. The ultimate goal of this research - individual estimates of water

65   volume stored in Sand Sea lakes - is important when evaluating aquatic habitats, conducting industrial activities that

require local freshwater supplies (i.e. ice road construction), and understanding regional water and energy balance.

Compared with lakes in surrounding regions of the ACP, Sand Sea lakes tend to be deeper and thus less likely to

freeze to the bottom during the winter. Their notable depth means that Sand Sea lakes tend to have lower

evaporative losses and are more likely to have basins characterized by floating (rather than bedfast) ice in the winter

70   (Arp et al. 2015; Engram et al., 2018). These unfrozen lake basins provide crucial overwintering habitat for fish and

other aquatic life (Jones et al., 2009; Sibley et al., 2008). Furthermore, liquid water is essential for industry during

winter, primarily for ice road construction, but also for ice airstrip and ice pad construction, exploratory oil-well

drilling, and withdrawal of water for drillers' and researchers' in-camp use (Jones et al., 2009). Unfrozen winter

lakes can also store more heat, affecting the regional energy balance (Jeffries et al., 1999). Therefore, depth and

75   volume quantifications of deep Sand Sea lakes can help monitor fish habitat and direct locations of water extraction

for wintertime infrastructure and consumption for other purposes.

       Previous studies have evaluated water depth and bathymetry of lakes in nearby regions using various

methods, but are limited either to shallow lakes or by coarse depth resolution (e.g. Hinkel et al., 2012; Jeffries et al.,

1996; Jones et al., 2017; Kozlenko and Jeffries, 2000; Sellman et al., 1975). Such limitations make deep lake depth

80   and volumetric estimation unfeasible. For example, Jeffries et al. (1996) used satellite imagery and radar data to

determine which lakes in regions near Utqiaġvik (Barrow) and Atqasuk, Alaska (including lakes in this paper's study area) froze to the bottom during the winter, extrapolating from their results a classification of lakes as being less than or greater than 2.2 m deep. When used in concert with an ice-growth model, this provided a proxy for coarse lake volume estimation, but was limited to shallow lakes. Hinkel et al. (2012) measured in situ bathymetry

85   for 28 lakes. However, the maximum lake depth of this study on the inner ACP was 2.3 - 5.2 m. Thus, our dataset and study is unique in its consideration of deep lakes. Furthermore, while one of the model variants we test was successfully used to extrapolate bathymetry in tropical and sub-tropical coastal marine environments (Jagalingam et al., 2015; Stumpf et al., 2003), to our best knowledge, the model has never been applied to high Arctic lakes. Volumetric estimates with the resolution provided here (30 m horizontal; 0.03 m vertical) have never been attempted

90   for Pleistocene Sand Sea lakes and the method of depth derivation used in this paper has not been employed in the Arctic.

2 Methods

2.1 Field methods

95   Depth points were sampled across 19 lakes during a field expedition between 22 July 2017 and 27 July 2017. The method of data collection required landing on each target lake in a float plane. A HumminBird 798ci HD SI Combo automatic sonar unit was attached to the back of a float and taxied or drifted across the lake. Depth points were each measured discretely as part of a depth-gradient transect, and were accurate to 0.03 m (due to intrinsic machine error).

100   Lakes were targeted that were large enough for a float plane to land on in windy conditions (i.e. > ~1 km^2 lake surface area), and showed the presence of a distinct littoral shelf and a deep basin on 2.5-m color-infrared aerial photography (U.S. Geological Survey Digital Orthophoto Quadrangles [DOQs]). Transect lines were mapped to encompass a wide depth range, however due to windy conditions, such lines were not always followed. Nevertheless, in all but two lakes, a depth range from the littoral shelf to the deep central basin was captured.

105

2.2 Depth data processing

     Depth data points from 17 of the 19 sampled lakes were compiled into a single file. Two lakes at which sampling occurred contained an insufficient number of measurements to justify modeling their bathymetry. Top-of-Atmosphere (TOA) reflectance values from the blue band (band 2; 452 - 512 nm), green band (band 3; 533 - 590

110   nm), and red band (band 4; 636 - 673 nm) of the Landsat image (described in the section below) were extracted to each point. The coastal band (band 1; 435 - 451 nm) was not included here as there is no basis for its examination in prior similar studies (e.g. Jagalingam et al., 2015) and preliminary results were not improved by the inclusion of the coastal band.

     The dataset was filtered to 13,735 depth points: for each transect collected with the HumminBird sonar,

115   discrete points were evaluated relative to the depths of their neighbors and anomalous and zero depth points were manually removed from the dataset. This improved the smoothness of the bathymetric profiles that were generated from each transect. Subsequently, depths collected at the margins of two lakes at the Pik Dunes (70.234 °N, 153.183

color of the sandy substrate at this group of lakes and the extreme shallow nature of the littoral shelves (~ 0.5 m

120   deep) produces a spectral signature near the margins of lakes in the Pik Dunes area that is easily confused with that
of the surrounding land and thus should not be used to analyze lake depth.

To minimize error caused by associating a single pixel's spectral signature with multiple depth points (i.e.
to reduce compatibility issues between the spatial resolution of the sonar transects and Landsat imagery to which the
depth points were compared), the dataset was degraded to include only one depth per pixel. This depth was

125   calculated by averaging the sonar depths of all measurements within the pixel, removing depths greater than one
standard deviation from this average, and re-calculating the depth mean of the pixel. This pixel-representative depth
point provides the final depth value used in analysis.

2.3 Landsat image selection, processing, and analysis

130   Landsat-8 Operational Land Imager (OLI) imagery was chosen for comparison with measured depth data
due to its large swath, 30-m spatial resolution, and quality (as assured by U.S. Geological Survey pre-processing). A
cloud-free Landsat image (LC08_L1TP_077011_20160805_20170222_01_TI) was selected that both covered the
study area and was acquired on 5 August 2016, that is, at a similar time of year to that of field data collection from
the following year. The late summer was chosen to provide data for a time when lakes are at an intermediate level,

135   that is, lakes are free of ice, but have not yet reached their lake level minimums (determined when evaporation
exceeds precipitation; Jones et al., 2009). It should be noted that water volume varies seasonally and interannually in
accordance with precipitation of the preceding twelve months, and therefore the estimated depth data may not be
representative of the lake levels year round or from year-to-year. Nevertheless, these variations in lake level are
relatively small, with surface area changes often around 0.6% of total surface area (Jones et al., 2009). Furthermore,

140   of these area changes, the majority of change occurs at the shallow littoral shelves and therefore results in little
volume change (Jones et al., 2009).

As no ice-free, cloud-free Landsat images exist that cover all study lakes for late summer 2017, we selected
a Landsat image from 2016 in order to maximize the number of lakes included at which field data exists, i.e. the
number of lakes at which we could model volume. One potentially promising Landsat image exists that covers our

145   study area, however (a) it was acquired at the end of June, just after ice out, when the lake levels are at a seasonal
high, and (b) slight cloudiness over some study lakes produced models that predicted depths up to 48% less
accurately. The use of 2016 imagery is further justified as the interannual depth and volume changes are smaller
than our error metrics. When considering one representative lake (located at 70.147 °N, 151.765 °W), a continuous
depth logger recorded a depth difference of 0.03 m (or 1% of the annual average depth at that point) between the

150   imagery acquisition date (5 August 2016) and the time of data collection (26 July 2017). This represents a smaller
depth difference than the 0.05 m difference measured between 30 June 2017 and 26 July 2017. The maximum
observed depth change at this location between 1 January 2016 and 26 July 2017 was on the order of 1 m.
Observation of an imagery timeseries of a different group of lakes that are typically highly responsive to water level
changes (located at 70.539 °N, 152.733 °W) similarly revealed lake level conditions to be more comparable between

155   5 August 2016 and 21–27 July 2017 than between these latter dates and 1 July 2017. Overlaying lake surface area

changes on an airborne LiDAR-derived digital surface model showed a change in water level of ~ 0.10 m between 5

August 2016 and 1 July 2017, indicating a depth change well within our error margins (Alaska North Slope LiDAR

Data - Project Code ALCC2012-05). The chosen Landsat image

(LC08_L1TP_077011_20160805_20170222_01_TI) was clipped to the study area and a Normalized Difference

160   Water Index (NDWI) water mask was created to subset our study lakes from the surrounding land pixels

(McFeeters, 1996).

        Study lakes were then visually assessed to provide a Boolean turbidity rating for the purpose of analyzing

the success of different models. Lake clarity was determined by comparing an RGB true color composite of the

Landsat image selected for analysis with a Landsat image acquired 13 July 2016 (23 days prior to the acquisition

165   date of the selected Landsat image), as well as color-infrared aerial photographs (DOQs) with a 2.5-m horizontal

resolution (Fig. 2). Lakes that showed presence of sediment plumes or water cloudiness near the site of in situ data

collection on the selected Landsat image were designated as turbid. Lakes which displayed minimal suspended

sediment distant from the area at which depths were recorded were designated as turbid as well, however they were

analyzed as if they were clear, as the impacts of sediment would not be seen in the depth point-derived spectral

170   signatures. Lakes that did not have sediment plumes were designated as clear.

2.4 Model application and volume estimation

        Twelve variations of a spectral-depth algorithm were examined, each characterized by a specific band ratio,

adjustment factor, and growth factor (Table 1). More specifically, the blue to green, blue to red, and green to red

175   band ratios were considered. Such ratios were either simple (e.g. blue band/green band) or transformed according to

Stumpf et al. (2003):

$$\frac{\ln(nR_i)}{\ln(nR_j)} \qquad\qquad (1)$$

        where R_i and R_j represent the TOA reflectances for bands i and j, respectively. A constant n is included to

effect a positive output (Stumpf et al., 2003). We set n to 500, as it ensured that the logarithm would be positive

180   given any feasible band value input, R, from our image.

        The band ratio and the depth measurement of the point at which the spectral signature was extracted were

correlated using either a linear regression or an exponential function (Fig. 3a-c). The constants obtained from each

of these models became the parameters with which to tune the linear or exponential equations for the validation data.

The root mean squared error (RMSE) of each regression between input depths and input band ratios provided error

185   statistics for modeled depths. In summary, the twelve model variations were each characterized by (1) one of three

band ratios, (2) one of two transformation methods, and (3) one of two growth relationships (Table 1).

        For each lake, half of the data was randomly selected as input data while the remaining data was used for

validation purposes. To ensure that the model was trained and validated with data spanning the full range of input

depths, however, the maximum and minimum depths were assigned to the group of data to input into the model,

190   while the second deepest and second shallowest depth points were retained in the list of validation data. To obtain

the best regional model, this same process was undertaken (i.e. random selection of half of the data to train the

models; application of each of the 12 models), however a sufficient number of depth points exist in the full dataset such that the explicit assignment of extreme depths values to input and validation data was unnecessary.

195   Each of the 12 models was tested at each of the 17 lakes and on a regional scale. To account for the slight variations in each model's capacity for depth prediction given different random sets of training data, 1,000 trials were performed. This allowed us to assert that the model designated as the most accurate model for a given lake (as determined from one trial) was the same model that most frequently produced the best results for that lake. The best model for each lake, as evaluated by the coefficient of determination between target and predicted data, was used to calculate depths at each pixel in that lake. Depths were multiplied by 900 m^2 (the area of one Landsat pixel) and

200   integrated to quantify the lake's water volume.

3 Results

The best models for lakes at which depth data were collected were able to account for 58.5% - 97.6% of depth variability (median $R^2 = 0.86$, mean $R^2 = 0.82$; Table 2). Regional-scale models, however, were able to

205   accurately explain less than half of the regional depth variability. Median uncertainty of single lake depth models (based on RMSE) was 1.23 m, while the average RMSE of the models was 1.44 m. However error was not distributed equally across depths, and models tended to overestimate shallower depths and underestimate deep depths (Fig. 3d-f). When considering model-predicted depths at all study lakes, depth points less than 2.95 m were overestimated by an average of 0.21 m (or 17.2% of their true depth), with 61.3% of depths in this shallow-water

210   group experiencing some model over-prediction. Meanwhile, 66.9% of depths greater than 2.95 m were underestimated, with an average difference between measured and modeled depths of 0.97 m. On average, points deeper than 2.95 m were underestimated by 5%. The threshold of 2.95 m represents the intersection between the 1:1 line and the correlation between measured and predicted depths. Coincidentally, approximately half of the data points used for model validation fall below this threshold.

215   Lake volumes ranged from 1.056 ×10^{-3} km^3 at the smallest lake (total surface area = 1.089 km^2) to 57.416 ×10^{-3} km^3 at the largest lake (total surface area = 18.998 km^2), with a median volume of 7.20 ×10^{-3} km^3 (Table 3). Volume and surface area were strongly correlated ($R^2 = 0.90$) for the 14 lakes at which complete volumes could be modeled (Fig. 4). Linear models predicted negative depths across much of the lakes' shallow littoral shelves; thus, the modeled volumes of the three lakes at which linear models produced the most accurate results are an incomplete

220   representation of the lake's water storage. Pixels at which models predicted negative depths were eliminated and the water volume was instead calculated for the surface area with predicted depths greater than zero (Fig. 5). Ground truth lake volume data do not exist for the study lakes at a similar scale of analysis, rendering error metrics unfeasible (aside from those implicitly contained in the depth model error).

The most accurate models (i.e. the models that were best able to determine lake depth for the greatest

225   number of lakes) were models with an exponential growth factor with input band ratios blue/green or blue/red (Table 2). In all but three of the study lakes, an exponential relationship was found between spectral signature and depth. At only two lakes did the green to red band ratio provide the best results. The transform ratio provided the best results in 4 out of the 17 lakes, while the simple ratio was used to best model depths in the remainder of the

lakes. The difference between the modeled results of the pure versus transform ratio was marginal however, with an

230 average difference between R^2 values generated by the respective models of 0.016.

Turbidity appears to partially explain band ratio success. All of the eight lakes at which the blue to green band ratio provided the best result were free of sediment where measurements were taken. Furthermore, all of the seven lakes designated as turbid at the data collection site required incorporation of the red band to achieve the best depth prediction. One anomalous lake at which no sediment was detected required incorporation of the red band to

235 predict depth most accurately.

4 Discussion

4.1 Modeled depth analysis

Depth was accurately derived from Landsat OLI imagery for individual lakes. Our R^2 values are consistent

240 with those found in the literature (e.g. Jagalingam et al., 2015; Stumpf et al., 2003) and thus our selected models can be considered successful. The regional scale model, however, was unsuccessful and regional volume analysis was rejected. This finding is consistent with Smith and Pavelsky (2009), who found surprisingly high variability in a collection of remotely sensed lake storage volumes on the Peace-Athabasca Delta, Canada, despite their having similar physiographic setting and morphology.

245 Unsurprisingly, the blue band proved to be the most useful in determining depth, and was used to tune depths at all but two lakes. Blue light has a shorter wavelength, and consequential higher energy, which allows it to be absorbed less in water than either green or red light. Thus, the reflectance of the blue band decreases less than either the green or red bands in proportion to increasing depth. In contrast, red light is able to penetrate only several meters into most types of water before it becomes absorbed. This band proved useful in distinguishing depths at both

250 the sandy littoral shelves, where water is typically 0.5 - 3 m in depth, and where suspended sediment was present in the water. As sand reflects red light more than blue or green light, this is expected. Thus, applying the blue to red band ratio to predict depths at turbid lakes, where sediment reduces blue and green wavelength penetration into deeper waters, is recommended. Conversely, applying the blue to green ratio at clear lakes where blue and green light can effectively penetrate water to the expected deeper depths will likely provide the best depth predictions.

255 However, it should be noted that the blue band is the most susceptible to contamination from atmospheric aerosols, which may contribute to the lack of model portability between lakes.

The two lakes at which the green/red band ratio best tuned the model were unique in terms of physical factors or sampling locations. One of these lakes showed the presence of an unusual purple-red patch on a shelf between the littoral shelf and deep zone. Underwater vegetation likely accounts for this unusual spectral signature

260 and thus it is unsurprising that this lake required a unique band ratio to accurately tune the model. Measurements at the second lake accounted for the shallowest range of depths of any lake (0.2 m - 2.1 m), which may have led to stronger reflectance in the red band, as the sand was more prominent.

In addition, an exponential relationship was able to better model depth ranges that include shallow depths of around 0.8 m, a finding that is likely the result of incomplete transect sampling rather than physical significance.

265 Of the three lakes at which a linear function provided the best model, two were the lakes at which depths on the

littoral shelf were not measured; the third lake contained only a single measurement of the littoral shelf. Therefore, the lakes best modeled with a linear growth relationship are associated with measured bathymetry profiles that do not contain sufficiently shallow littoral shelf depths. This is evidenced by the prediction of negative depths at littoral shelves when applying linear models, the product of the strongly negative y-intercepts that render low spectral

270   signature ratios negative. This leads us to conclude that the linear relationship between band ratios and depths at these lakes is more likely the product of the locations at which data was gathered rather than a result of physical significance. It is thus important to tune models to all regions (and all depths) of the lake.

On the whole, we found that applying an exponential function to compare depths to a simple band ratio provided the best accuracy, with model input bands dependent on physical factors specific to each lake. The simple

275   band ratio is easier to calculate and the accuracy provided by each ratio type model variant is comparable, with slightly better overall results when using the simple ratio. However, to address the underestimation of deep depths and overestimation of shallow depths in our models, additional transformations must be made, a goal that is outside the scope of this project.

280   4.2 Limitations

The depth estimates are only tuned to the extrema of depths measured at each lake. Although gathering data across a lake's full bathymetric profile was attempted, it is likely that the depth minima and maxima were not captured at all lakes. Collecting data with sonar attached to a float plane limited the measurement of depths approaching 0 m. Few pixels were sampled at the minimum depth that was able to be measured (0.2 m) and thus

285   there is insufficient tuning to accurately model the littoral shelves of lakes. Furthermore, while we attempted to gather depths across the deep central basins, it is impossible at present to know whether we sampled the deepest point without measuring the entirety of the basin. Thus, modeled depths may not accurately depict a lake's maximum depth.

The limited spatial resolution of Landsat imagery, in comparison with sonar depth data, constitutes the

290   primary limitation to this work. As depths had to be averaged to conform to the assumption that each spectral signature corresponded to a discrete depth, the spatial resolution and depth precision of the sonar depths was greatly degraded, potentially accounting for some of the inaccuracies in the model variants. Modeling bathymetry with satellite imagery of a higher spatial resolution would allow for the use of more training points and thus likely improve the accuracy of depth and volume predictions. Furthermore, samples were taken at a small fraction (in

295   terms of surface area) of the lake (i.e. the entire lake's bathymetry was not mapped, rather, data points were collected along discrete and irregular transects). Thus, there exists a mismatch regarding the validation data and the natural phenomenon being modeled. Data at such a small spatial scale can never confirm with total accuracy the detailed nature of lake bed bathymetry. Constrained by cost and time however, collecting data at 17 remote lakes is an important step towards understanding Sand Sea lake bathymetries on Alaska's Arctic Coastal Plain.

300

4.3 Implications and future directions

Lakes on the Pleistocene Sand Sea may be categorized based on depth, littoral substrate, and water clarity, as seen in the study lakes, with such categories providing candidates for different model variations. Future projects may use this work to semi-automatically derive depths across the region, first manually classifying target lakes, and

305   then applying different model variations to each class. Furthermore, subregions of each lake (e.g. deep basins, shallow shelves) may be classified in future studies and a different model variant applied to each subregion (e.g. variants that incorporate the red band applied to littoral shelves). Methods of lake subregion differentiation may include either (1) manual delineation based on spectral signatures or (2) automatic delineation with the aid of synthetic aperture radar (SAR) to determine regions of floating versus bedfast ice (which correspond with deep and

310   shallow water, respectively; demonstrated by Engram et al., 2018; Jeffries et al., 1996). Additional future work may include validation of lake water volumes as additional bathymetric datasets become available.

5 Conclusion

This work represents one successful application of leveraging in situ data collection with satellite remote

315   sensing to estimate lake water depth and volume. Lake volumes can be monitored using remote sensing, however at least one field visit must be made in order to select the best model for a given lake. As of yet, we do not have a way to universally model the bathymetry of lakes across northern Alaska. Instead, field data continues to be necessary to train and calibrate models on a per-lake basis.

320   **6 Data Availability**

We present a dataset to greatly increase the number of in situ measurements of lake depth on the little-studied Inner Arctic Coastal Plain of Alaska. The dataset contains 13,735 point measurements of bathymetric depth measured across 19 lakes, and is freely available through the National Science Foundation Arctic Data Center: https://doi.org/10.18739/A2SN01440 (Simpson and Arp, 2018). The second dataset created for this project is

325   comprised of 17 bathymetry rasters, one for each lake at which a sufficient number of depth points was collected. These rasters represent the depth predictions of the best performing model for each individual lake and are also freely available through the National Science Foundation Arctic Data Center: https://doi.org/10.18739/A2TQ5RD83 (Simpson, 2019).

330   **Author contributions**

Claire E. Simpson and Christopher D. Arp designed the sampling. Christopher D. Arp secured the funding and instrumentation for field work. Claire E. Simpson, Christopher D. Arp, and Benjamin M. Jones conducted the field work. Claire E. Simpson processed and analyzed the data and prepared the figures and tables. Claire E. Simpson prepared the manuscript with contributions from all co-authors.

335

Competing interests

The authors declare that they have no conflict of interest.

Acknowledgements

340   This research was supported by the National Sciences Foundation, NSF Project #1560372, REU: Understanding the Arctic as a System, NSF Project #1417300, ALISS: Arctic Lake Ice Systems Science (www.arcticlakeice.org), NSF Project #1806213, and the Bureau of Land Management Arctic District Office. Additional funding for this project was provided by the NASA Arctic-Boreal Vulnerability Experiment (ABoVE) grant NNX17AC60A to L.C.S., and the University of California, Los Angeles Honors Program's Irving and Jean

345   Stone Research Award. Special thanks to Jim Webster for flight support.

350

References

Alaska North Slope LiDAR Data (Project Code ALCC2012-05), Arctic Landscape Conservation Cooperative, [online] Available from: http://arcticlcc.org/projects/geospatial-data/alaska-north-slope-lidar-data (Accessed 30 October 2018), n.d.

355   Arp, C. D., Jones, B. M., Liljedahl, A. K., Hinkel, K. M. and Welker, J. A.: Depth, ice thickness, and ice-out timing cause divergent hydrologic responses among Arctic lakes, Water Resources Research, 51(12), 9379–9401, doi:10.1002/2015WR017362, 2015.

Carson, C. E.: Radiocarbon Dating of Lacustrine Strands in Arctic Alaska, Arctic, 21(1), 12–26, 1968.

360

Carson, C. E. and Hussey, K. M.: The Oriented Lakes of Arctic Alaska, The Journal of Geology, 70(4), 417–439, doi:10.2307/30063413, 1962.

Carter, L. D.: A Pleistocene Sand Sea on the Alaskan Arctic Coastal Plain, Science, 211(4480), 381–383,

365   doi:10.1126/science.211.4480.381, 1981.

Engram, M., Arp, C. D., Jones, B. M., Ajadi, O. A. and Meyer, F. J.: Analyzing floating and bedfast lake ice regimes across Arctic Alaska using 25 years of space-borne SAR imagery, Remote Sensing of Environment, 209, 660–676, doi:10.1016/j.rse.2018.02.022, 2018.

370

Hinkel, K. M., Frohn, R. C., Nelson, F. E., Eisner, W. R. and Beck, R. A.: Morphometric and spatial analysis of thaw lakes and drained thaw lake basins in the western Arctic Coastal Plain, Alaska, Permafrost Periglac. Process., 16(4), 327–341, doi:10.1002/ppp.532, 2005.

Hinkel, K. M., Sheng, Y., Lenters, J. D., Lyons, E. A., Beck, R. A., Eisner, W. R. and Wang, J.: Thermokarst Lakes

375   on the Arctic Coastal Plain of Alaska: Geomorphic Controls on Bathymetry, Permafrost and Periglac. Process.,

23(3), 218–230, doi:10.1002/ppp.1744, 2012.

Hopkins, D. M.: Thaw Lakes and Thaw Sinks in the Imuruk Lake Area, Seward Peninsula, Alaska, The Journal of

Geology, 57(2), 119–131, doi:10.1086/625591, 1949.

380

Jagalingam, P., Akshaya, B. J. and Hegde, A. V.: Bathymetry Mapping Using Landsat 8 Satellite Imagery, Procedia

Engineering, 116, 560–566, doi:10.1016/j.proeng.2015.08.326, 2015.

Jeffries, M., Zhang, T., Frey, K. and Kozlenko, N.: Estimating late-winter heat flow to the atmosphere from the

385   lake-dominated Alaskan North Slope, Journal of Glaciology, 45, 315–324, doi:10.3189/002214399793377095,

1999.

Jeffries, M. O., Morris, K. and Liston, G. E.: A Method To Determine Lake Depth and Water Availability on the

North Slope of Alaska with Spaceborne Imaging Radar and Numerical Ice Growth Modelling, ARCTIC, 49(4),

367–374, doi:10.14430/arctic1212, 1996.

390   Jones, B. M., Arp, C. D., Hinkel, K. M., Beck, R. A., Schmutz, J. A. and Winston, B.: Arctic Lake Physical

Processes and Regimes with Implications for Winter Water Availability and Management in the National Petroleum

Reserve Alaska., Environmental Management, 43(6), 1071–1084, 2009.

Jones, B. M., Arp, C. D., Whitman, M. S., Nigro, D., Nitze, I., Beaver, J., Gädeke, A., Zuck, C., Liljedahl, A.,

Daanen, R., Torvinen, E., Fritz, S. and Grosse, G.: A lake-centric geospatial database to guide research and inform

395   management decisions in an Arctic watershed in northern Alaska experiencing climate and land-use changes,

Ambio, 46(7), 769–786, doi:10.1007/s13280-017-0915-9, 2017.

Jorgenson, M. T. and Shur, Y.: Evolution of lakes and basins in northern Alaska and discussion of the thaw lake

cycle, J. Geophys. Res., 112(F2), F02S17, doi:10.1029/2006JF000531, 2007.

400

Jorgenson, M. T., Kanevskiy, M., Shur, Y., Grunblatt, J., Ping, C. L., and Michaelson, G.: Permafrost database

development, characterization, and mapping for northern Alaska. Report for Arctic Landscape Conservation

Cooperative by Alaska Ecoscience and University of Alaska Fairbanks (45 pp.,

http://www.gina.alaska.edu/projects/permafrostdatabase-and-maps-for-northern-alaska) (2014).

405   Kozlenko, N. and Jeffries, M. O.: Bathymetric Mapping of Shallow Water in Thaw Lakes on the North Slope of

Alaska with Spaceborne Imaging Radar, ARCTIC, 53(3), 306–316, doi:10.14430/arctic860, 2000.

Livingstone, D. A.: On the orientation of lake basins [Alaska], Am J Sci, 252(9), 547–554, doi:10.2475/ajs.252.9.547, 1954.

410

McFeeters, S. K.: The use of the Normalized Difference Water Index (NDWI) in the delineation of open water features, International Journal of Remote Sensing, 17(7), 1425–1432, doi:10.1080/01431169608948714, 1996.

Rex, R. W.: Hydrodynamic Analysis of Circulation and Orientation of Lakes in Northern Alaska, Defense Technical

415   Information Center, 1961.

Sellman, P. V., Brown, J., Lewellen, R. I., McKim, H. and Merry, C.: The Classification and Geomorphic Implications of Thaw Lakes on the Arctic Coastal Plain, Alaska, Research Report, Cold Regions Research and Engineering Lab, Hanover, NH, 1975.

420   Sibley, P. K., White, D. M., Cott, P. A. and Lilly, M. R.: Introduction to Water Use From Arctic Lakes: Identification, Impacts, and Decision Support1, JAWRA Journal of the American Water Resources Association, 44(2), 273–275, doi:10.1111/j.1752-1688.2007.00159.x, 2008.

Simpson, C. and Arp, C.: Sonar Depth Measurements at Lakes on the Inner Arctic Coastal Plain of Alaska, July 2017, Arctic Data Center, doi:10.18739/A2SN01440, 2018.

425

Simpson, C.: Modeled Bathymetry Maps of 17 Lakes on the Arctic Coastal Plain of Alaska, 2017, Arctic Data Center, doi:10.18739/A2TQ5RD83, 2019.

 Smith, L. C. and Pavelsky, T. M.: Remote sensing of volumetric storage changes in lakes, Earth Surf. Process.

430   Landf., 34(10), 1353–1358, doi:10.1002/esp.1822, 2009.

Stumpf, R. P., Holderied, K. and Sinclair, M.: Determination of water depth with high-resolution satellite imagery over variable bottom types, Limnology and Oceanography, 48(1), 547606, 2003.

van Everdingen, R.: Multi-language glossary of permafrost and related ground-ice terms, Natl. Snow and Ice Data

435   Cent., Boulder, Colo., 1998.

Williams, J.R.: Engineering - geologic maps of northern Alaska, Meade River Quadrangle: U.S. Geological Survey Open-File Report 83-294, 29 p., 1 sheet, scale 1:250,000,1983.

Williams, J. R., Carter, L. D., and Yeend, W. E.: Coastal Plain Deposits of NPRA, The United States Geological Survey in Alaska, Accomplishments During 1977, U.S. Department of the Interior, Geological Survey., 1978.

440

Tables

Table 1: Modeled depth (Z) is calculated with each of four equations that are tuned with each of three input band pairs. R_i and R_j represent the Top-of-Atmosphere reflectances of bands i and j, respectively. Band pairs (band i/band j) include the blue and red bands, the blue and green bands, and the green and red bands. Tunable parameters m_1 and m_0 are derived by comparing spectral signatures with depth (as in Fig. 3a-c).

		Ratio adjustment type	
		Transform	Simple
Growth factor	Linear	$Z = m_1\left(\dfrac{\ln(nR_i)}{\ln(nR_j)}\right) - m_0$	$Z = m_1\left(\dfrac{R_i}{R_j}\right) - m_0$
	Exponential	$Z = m_0 e^{m_1\left(\frac{\ln(nR_i)}{\ln(nR_j)}\right)}$	$Z = m_0 e^{m_1\left(\frac{R_i}{R_j}\right)}$

450 **Table 2: The best spectral depth model for each lake (based on R^2).** A simple ratio exponential function provided the best model for the greatest number of lakes, while the blue/green and blue/red band ratios both provided good inputs for models at different lakes, accounting for the best spectral-depths models at 8 and 7 lakes, respectively. The average R^2 of the best model at each lake is 0.818, with an average root mean squared error (RMSE) of 1.439 m. *Some suspended sediment is visible, however it does not approach the area at which depths were measured.

Lake ID	Centroid latitude (dd)	Centroid longitude (dd)	Measured depth range (m)	Turbid?	Ratio type	Best method		R^2	RMSE
						Band ratio	Growth type		
2964	70.3616	-153.6750	1.6 - 11.5	No	Transform	Blue/Green	Linear	0.802	1.973
3442	70.3168	-153.8160	0.8 - 2.3	Yes	Simple	Green/Red	Exponential	0.916	0.270
3839	70.2875	-153.8620	1.7 - 6.1	Yes	Simple	Blue/Red	Exponential	0.871	0.600
4199	70.2457	-154.4680	1.3 - 12.7	No	Simple	Blue/Green	Exponential	0.632	2.132
4222	70.2484	-153.1460	0.2 - 11.7	Yes	Simple	Blue/Red	Exponential	0.689	2.307
4291	70.2386	-153.2030	2.7 - 6.1	Yes	Simple	Blue/Red	Exponential	0.585	0.835
4365	70.2304	-153.2500	0.4 - 4.8	No	Simple	Blue/Green	Linear	0.784	0.478
4782	70.1983	-153.3150	0.2 - 2.1	Yes	Transform	Green/Red	Exponential	0.893	0.138
5211	70.1581	-153.9300	0.7 - 5.0	Yes	Simple	Blue/Red	Exponential	0.804	0.563
5242	70.1585	-154.2260	2.1 - 8.2	Yes*	Simple	Blue/Green	Exponential	0.976	0.684
5326	70.1349	-154.1280	0.7 - 4.4	No	Simple	Blue/Red	Exponential	0.862	0.425
5570	70.0948	-153.7480	0.8 - 10.0	No	Simple	Blue/Green	Exponential	0.654	1.957
5893	70.0577	-153.5010	0.3 - 21.0	Yes*	Transform	Blue/Green	Exponential	0.954	1.931
6058	70.0285	-153.3670	0.6 - 17.0	No	Simple	Blue/Green	Exponential	0.866	3.568
6167	70.0122	-153.0930	0.8 - 14.2	Yes*	Transform	Blue/Green	Exponential	0.848	2.604
6199	70.0110	-153.4720	2.2 - 10.5	Yes	Simple	Blue/Red	Linear	0.907	1.227
6274	69.9967	-153.0690	0.5 - 13.0	Yes*	Simple	Blue/Red	Exponential	0.867	2.765

455

Table 3: Modeled Lake Volumes. Individual lake volumes were estimated by multiplying the modeled depth for each pixel by a constant factor of 900 m^2 (Landsat spatial resolution). Depths were modeled by applying the best spectral-depth model for the lake (Table 2). Linear depth models predicted negative depths for some pixels; volume estimates derived from such models (namely the models applied at lakes 2964, 4365, and 6199) include only those pixels with modeled depths greater than zero. The percent of the surface area for which depth estimates at a lake were positive (in contrast to the total surface area of a given lake derived using the NDWI mask) is quantified.

Lake ID	Total surface area (km^2)	Surface area with depths modeled (% total area)	Modeled volume (10^{-3} km^3)
2964	4.631	25.78	11.113
3442	1.089	100	1.056
3839	5.419	100	10.367
4199	1.953	100	3.454
4222	1.533	100	8.371
4291	0.637	100	2.229
4365	1.046	61.66	2.102
4782	6.455	100	7.202
5211	9.865	100	19.280
5242	18.998	100	57.416
5326	4.846	100	10.545
5570	0.913	100	2.464
5893	10.552	100	37.949
6058	1.559	100	6.336
6167	2.778	100	10.343
6199	2.038	37.24	4.943
6274	0.662	100	2.484

460

465

470

475

Figures
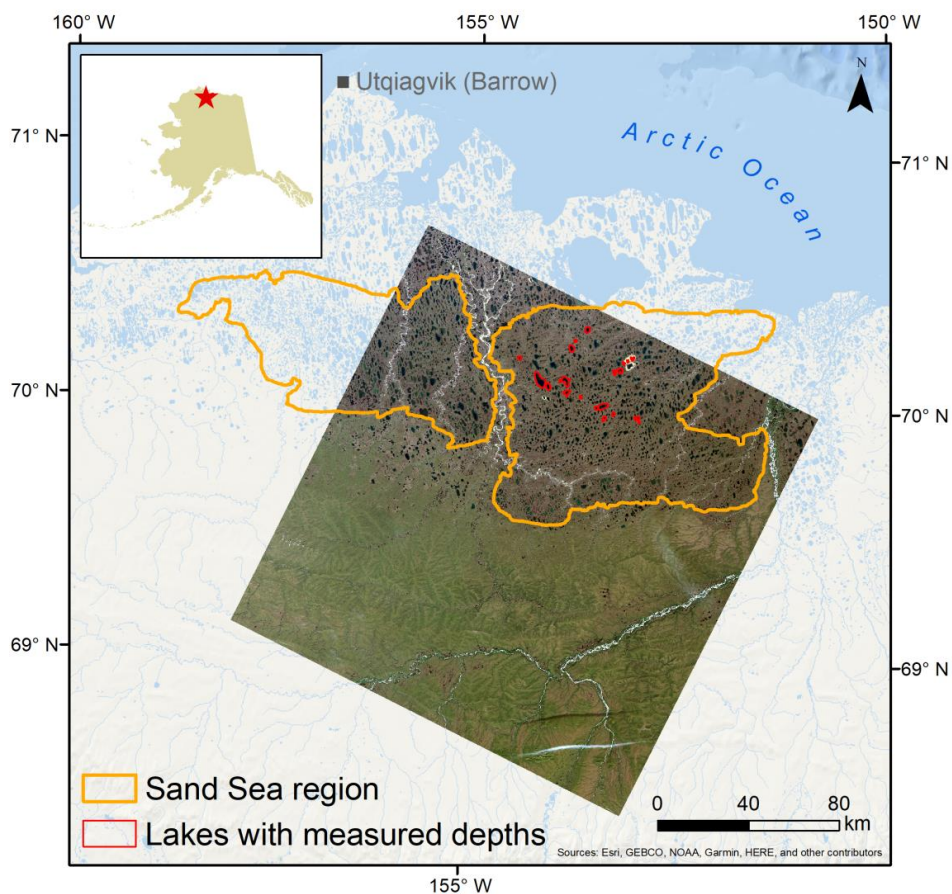
480

Figure 1. The lake-rich region of study is on Alaska's Arctic Coastal Plain (ACP), southeast of Utqiaġvik (Barrow). The imagery
used in our models is a Landsat-8 tile (Path 077, Row 011) acquired on 5 August 2016. The Pleistocene Sand Sea, a geologically-
unique region of the ACP, is delineated based on a classification of eolian sand by Jorgenson et al., 2014. Landsat-8 image
courtesy of the U.S. Geological Survey.

485
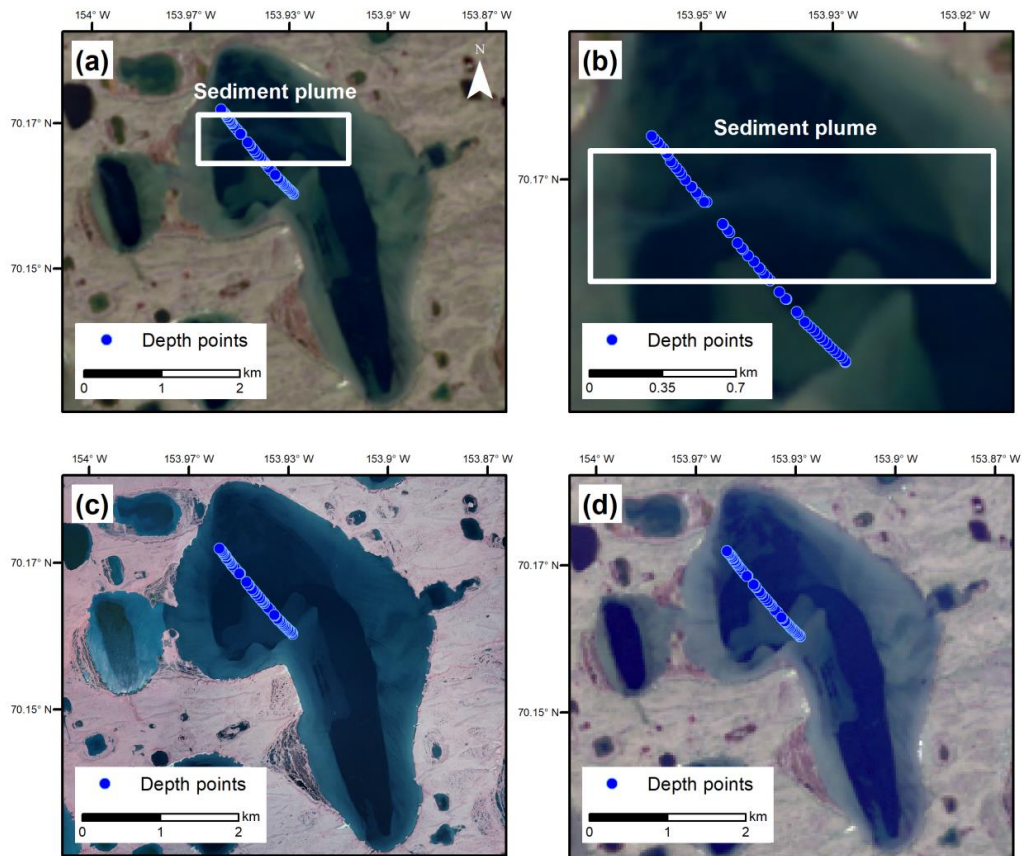
Figure 2. Sediment is detected in RGB Landsat imagery (acquired 5 August 2016) of a representative study lake **(a,b)**. This is confirmed as a temporary sediment plume by comparing the image of the lake used in modeling to 2.5-m color-infrared
490   photography acquired 18 July 2002 **(c)** and a Landsat image acquired 13 July 2016 **(d)** in which no sediment plumes are visible. Landsat-8 images and Digital Orthophoto Quadrangles (DOQs) courtesy of the U.S. Geological Survey.
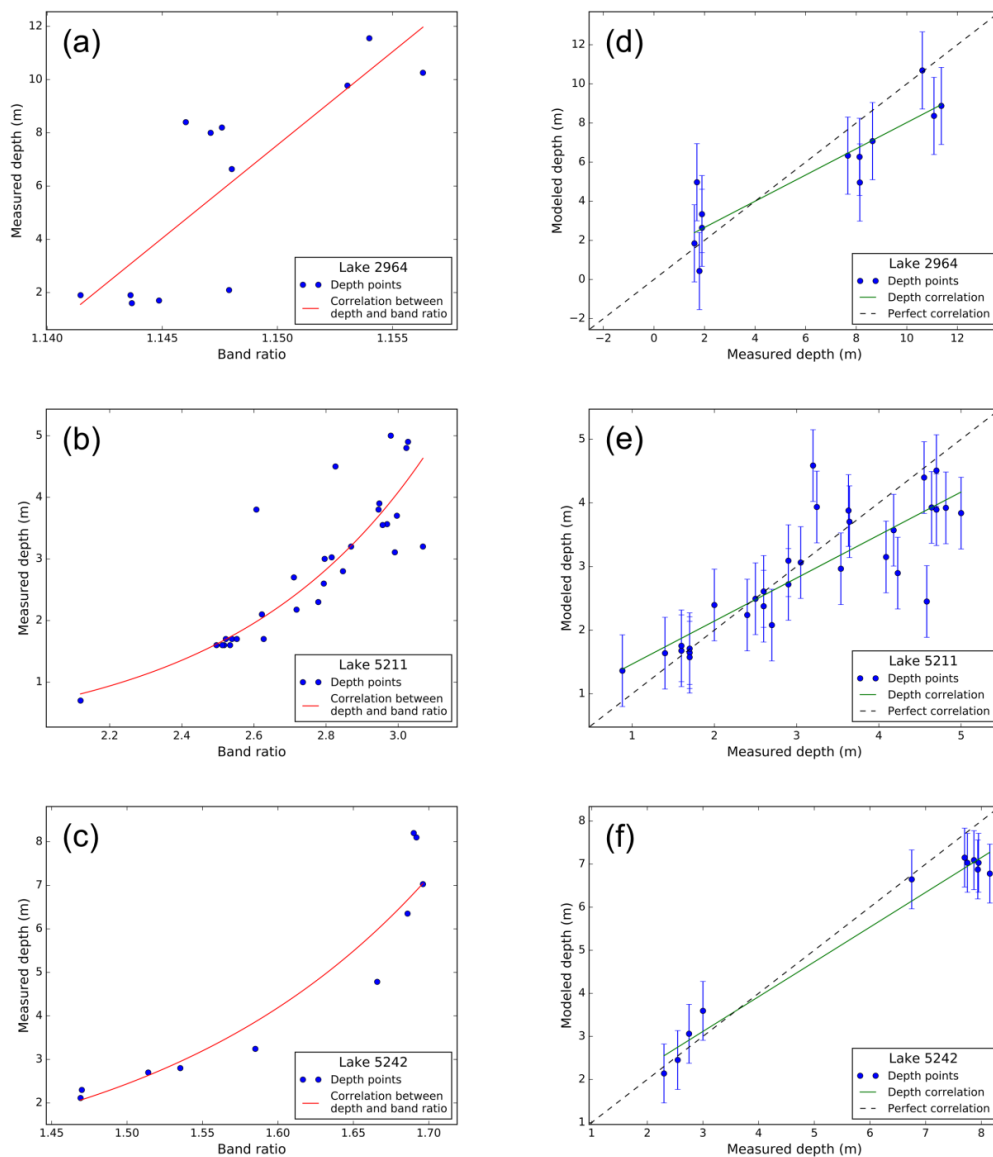
Figure 3. Coefficients of the trendlines between band ratios and measured depths **(a-c)** are used to tune the depth models for each
lake. Different models (specified for each lake in Table 2) best predicted lake depth at each of these three lakes. Correlation
between measured and modeled lake depths at three representative lakes **(d-f)** reveals underestimation of deeper depths and
overestimation of shallow depths. Error bars represent root mean squared error (RMSE).
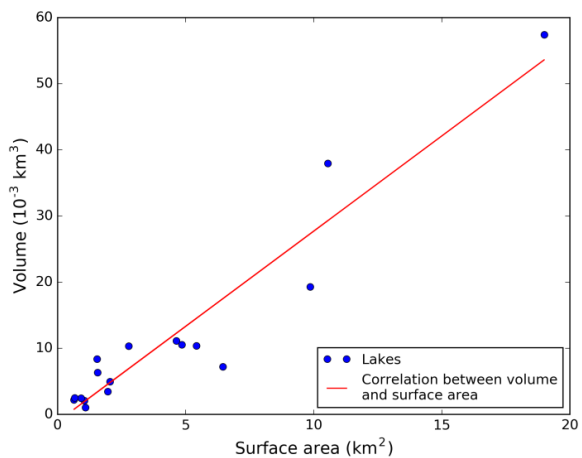
500   **Figure 4.** A strong correlation exists between surface area and modeled volume for the 17 lakes we analyzed.
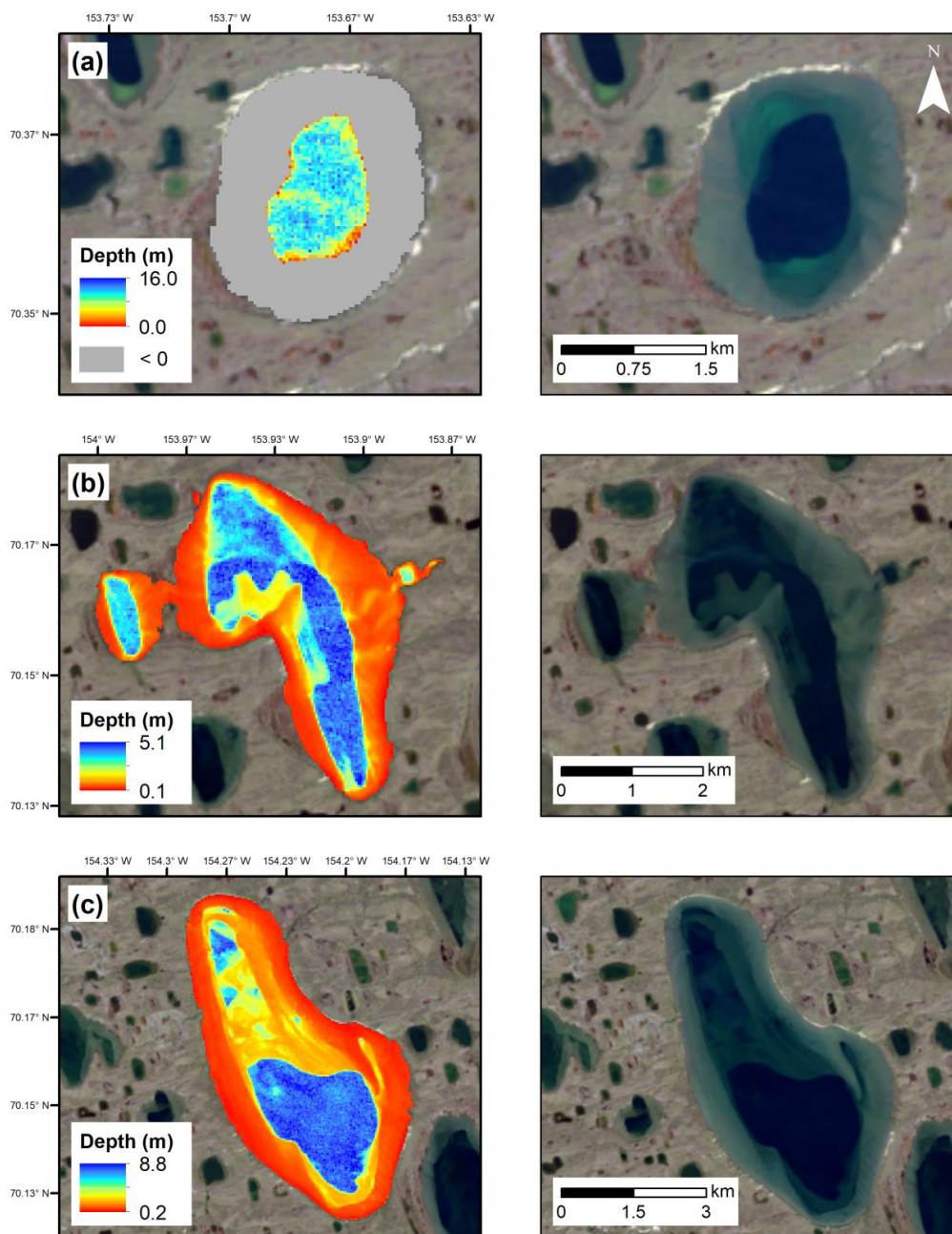
Figure 5. Modeled lake bathymetry at three representative lakes reveals the tendency of linear depth models to drastically underestimate the depths of the littoral shelves when not calibrated to shallow depths **(a)** and the promising predictive power of

505 exponential depth models **(b,c)**. The products of three different spectral-depth model variations are overlain on the Landsat

imagery from which the products were derived. Adjacent to each depth product is the original Landsat imagery of the lake. Color

bars indicate the depths predicted by the model variants at each lake, while the grey area **(a)** represents the pixels at which

negative depths were modeled. Landsat-8 image courtesy of the U.S. Geological Survey.

510

515

520

525

530